Range Measurement based Localization between Mothership and Lander Considering Asteroid Shape Using Particle Filter

By Hirokazu ISHIDA,[1)] Yuichi TSUDA,[2)]

[1)]*Department of Aeronautics and Astronautics, The University of Tokyo, Tokyo, Japan*
[2)]*Institute of Space and Astronautical Science, JAXA, Sagamihara, Japan*

(Received June 21st, 2017)

The in-situ exploration using asteroid landers is an attracting idea in the asteroid exploration. As a localization method for these landers, there have been proposed a conventional method based on the range measurement between the lander and its mothership. However, this conventional method provides low accuracy localization in the case when the mothership moves only slightly during the observation. To improve the drawback of the conventional method, we develop it by taking into account the constraints that the lander exists on the asteroid surface. We express this constraint by using particle filters. According to the simulation results, the proposed method provides much better performance than the conventional method.

Key Words: Asteroid Surface, Range Measurement, Particle Filter, Merging Particle Filter

Nomenclature

ζ or $\boldsymbol{\zeta}$	:	measurement value (scalar or vector)
w or $\boldsymbol{w}$	:	measurement noise (scalar or vector)
$\boldsymbol{X} = [X, Y, Z]^T$	:	position of lander
$\boldsymbol{x} = [x, y, z]^T$	:	position of mothership
$\dot{\boldsymbol{x}} = [\dot{x}, \dot{y}, \dot{z}]^T$	:	velocity of mothership
$\boldsymbol{s} = [\boldsymbol{X}^T, \boldsymbol{x}^T, \dot{\boldsymbol{x}}^T]^T$	:	state vector
r	:	norm of $\boldsymbol{x}$
$\boldsymbol{R}$	:	rotation matrix
N	:	number of particles
n	:	number of sub-ensembles
σ	:	standard deviation
Σ	:	covariance matrix
N_τ	:	threshold used in PF
m_p	:	parameter of MPF
t	:	time
Subscripts		
rm	:	range measurement
c	:	camera
0	:	initial
k	:	time step k
$k+1\|k$	:	forecast estimation
$k+1\|k+1$	:	filtered estimation

1. Introduction

Asteroid exploration has been attracting many space agencies in the world. The idea of performing the in-situ observation by the asteroid lander (or rover) has been proposed.[1,2)] In order to exploit the scientific data obtained by the landers, accurate localization of the asteroid lander is essential. Also, some landers that have hopping mechanism, such as MINERVA, MINERVA2, Hedgehog, and MASCOT, have been proposed.[1–3)] For these landers accurate localization is necessary for their navigation.

There have been proposed a method for lander localization using Kalman Filter based on the range measurement between the lander and its mothership.[4)] The key point of this approach is that the rover is rotating on the spinning asteroid and the mothership is orbiting around the asteroid. Due to their motions, there are many different positional relationships between the lander and mothership as shown in Fig. 1(left). By obtaining the multilateral information from the different positional relationships, this method works as same as the GPS and achieves the accurate localization in all directions, although this method relies only on one-dimensional measurement.

However, this conventional method does not always work well. The fairly realistic but difficult situation for this method is the hovering operation. Unlike the orbiting operation under strong perturbation, the hovering operation is relatively safe. Therefore, the hovering operation was chosen as a nominal operation by actual asteroid exploration missions.[1,5)] In the hovering operation, the spacecraft keeps its relative position to the asteroid by periodic delta-V at a distance of 10 to 20 km. The reason why the conventional method does not work well in this situation is that the change of the measurement direction of the lander from the mothership is little during the observation as shown in Fig. 1(right). Therefore, the localization accuracy of the directions except the measurable single direction becomes low. Of course, similar situations occur even in the orbiting operation if the orbital period is long.

In order to make the conventional method applicable in general cases, this paper proposes a filtering method that takes into account the asteroid shape. The precise asteroid shape can be obtained as polygonal data, for example, in Hayabusa mission.[6)] By considering the constraint that the lander exists on the asteroid surface, the localization is considered to converge more quickly than by the conventional method. Since the probabilistic density function (PDF) of the lander position on the asteroid surface is highly non-Gaussian, we use the Particle Filter (PF).

To evaluate the superiority of the proposed method over the conventional method, we performed simulations. The parameters of the mothership and asteroid are set to be those of "Hayabusa 2" and "Ryugu", respectively, and we assume the mothership is in the hovering operation. This setting is realistic

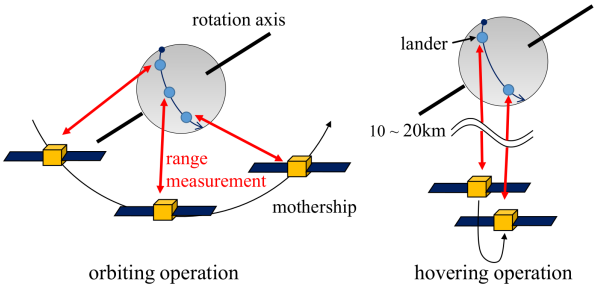

Fig. 1. Orbiting operation (left) and hovering operation (right) with range measurement between the mothership and lander.

Table 1. Physical parameters of Ryugu.[9,10]

Radius ρ	435 m
Gravitational constant μ	32 m^3/s^2
mean motion n	$1.53 \times 10^{-}7\mathrm{m/s^2}$
Rotation velocity ω	2.3×10^{-4} rad/s
Spin axis $(\lambda_{ecl}, \beta_{ecl})$	$(20°, 330°)$

because Hayabus 2 actually has 4 landers (or rovers), and they have function of range measurement between the themselves and their mothership Hayabusa 2.[7)]

We begin in Section 2 with an introduction of the dynamics and observation model of both the lander and mothership. In Section 3, we describe the proposed method using the PF. We performed simulation in Section 4, and then compare the performance of proposed and conventional methods.

2. Models

2.1. Motion model

In the following simulations the Hill coordinate system is used. The origin is set to the center of an asteroid. The $x-$, $y-$, and $z-$axes are set to be parallel to the direction from the sun to the asteroid, velocity vector of the asteroid, and angular momentum vector of the asteroid, respectively. The equation of motion of a mothership around the asteroid is written as follows,

$$\begin{aligned} \ddot{x} - 2n\dot{y} - 3n^2 x &= -\frac{\mu}{r^3}x + a_{srp} \\ \ddot{y} + 2n\dot{x} &= -\frac{\mu}{r^3}y \\ \ddot{z} + n^2 z &= -\frac{\mu}{r^3}z \end{aligned} \tag{1}$$

where the surface of the mothership is assumed to always face toward the sun, hence the solar radiation pressure is exerted along only the x-axis. a_{srp} is set to be $8.59 \times 10^{-8}\ \mathrm{m/s^2}$. These conditions about a_{srp} is set to be the same as Ref. 9). The equation of motion of the lander on the asteroid are written as follows,

$$\boldsymbol{X}_{k+1} = \boldsymbol{R}(\boldsymbol{a}, \omega\Delta t)\boldsymbol{X}_k \tag{2}$$

where $\boldsymbol{R}(\boldsymbol{a}, \omega\Delta t)$ is a rotation matrix around the axis $\boldsymbol{a}$ with the rotation angle $\omega\Delta t$. The parameters in Eq. (1) and Eq. (2) are set to be those of Ryugu. These physical parameters of Ryugu used in the following simulations are shown in Table 1. The relative positions of Ryugu and Earth to the sun and the spin axis are set by using ephemeris data at November 8th 2018.

2.2. Observation model

In the following simulations, the range measurement and camera-based asteroid direction measurement are assumed to be used. The latter one is used for the state estimation of the mothership. First, the observation equation of range measurement is written as follows,

$$\zeta_{rm} = h_{rm}(\boldsymbol{s}) = \|\boldsymbol{x} - \boldsymbol{X}\| + w_{rm} \tag{3}$$

where w_{rm} is a Gaussian noise with zero mean and standard deviation σ_{rm}. Second, the observation equation of camera-based asteroid direction measurement is written as

$$\boldsymbol{\zeta}_c = \boldsymbol{h}_c(\boldsymbol{s}) = [\tan^{-1}(x/y),\ \tan^{-1}(\sqrt{x^2 + y^2}/z)]^T + \boldsymbol{w}_c \tag{4}$$

where $\boldsymbol{w}_c$ is a Gaussian noise with zero mean and covariance matrix $\Sigma_c = \mathrm{diag}(\sigma_c^2, \sigma_c^2)$. Equation. (3) and Eq. (4) are set to be similar to the Ref. 4) and Ref. 11), respectively.

3. Localization method

3.1. Overview

In an actual situation, there is a constraint that the probability of the lander position is zero other than on the asteroid surface. On this constraint, the positional PDF of the lander becomes highly non-Gaussian. In this case, using the PF, which can be applied to any system, are appropriate.

The basic PF, however, are expected to not work well for the problem in this paper due to the problem called *sample impoverishment*. This problem is caused by repeating resamplings in the PF, through which particles converges to only high-likelihood states and particles become no longer able to approximate the real PDF. This phenomenon becomes remarkable in the following both cases: when the wide-range distribution expressed by particles is finally converged to the small-range and when process noise in the system is small/nothing. In this paper, the initial distribution of the lander spread to a wide range and converged to the much smaller region. Also, the system in this paper has no process noise as shown in Eq. (1) and Eq. (2). Thus, in this problem, simply applying PF is not sufficient.

In order to avoid this problem, a sample-impoverishment-resistant particle filter named Merging Particle Filter (MPF) is used in the following simulation.[8)]

3.2. Basic particle filter

The PF is a method that uses many particles to approximate a PDF. Thus, the PF is applicable to estimation problems with nonlinear systems and non-Gaussian noise. Consider the system as follows,

$$\boldsymbol{s}_{k+1} = \boldsymbol{f}_k(\boldsymbol{s}_k, \boldsymbol{v}_k), \tag{5}$$

$$\boldsymbol{\zeta}_k = \boldsymbol{h}_k(\boldsymbol{s}_k, \boldsymbol{w}_k). \tag{6}$$

The algorithm of the PF is divided into the following two steps: the forecast step and filtering step, which correspond to the propagation step and the measurement update step of the Kalman Filter, respectively.

· Forecast step

Forecast means transferring particles according to the state equation. By using $\boldsymbol{f}_k$, the N particles of the filtered ensemble at time k, are transferred to particles of the forecast ensemble at time $k+1$, which are expressed as follows,

$$\boldsymbol{s}_{k+1|k}^{(i)} = \boldsymbol{f}_k(\boldsymbol{s}_{k|k}^{(i)}, \boldsymbol{v}_k) \ \ (1 \le i \le N). \tag{7}$$

· Filtering step

Filtering step consists of the following two steps. First, calculate the likelihoods of particles $\{P(\boldsymbol{z}_{k+1}|\boldsymbol{s}_{k+1|k}^{(i)})\}_{i=1}^{N}$ and compute

$$^{*}w_{k+1}^{(i)} = w_k^{(i)} P(\boldsymbol{\zeta}_{k+1}|\boldsymbol{s}_{k+1|k}^{(i)}) \ \ (1 \le i \le N). \tag{8}$$

then regularize them as follows,

$$w_{k+1}^{(i)} = \frac{^{*}w_{k+1}^{(i)}}{\sum_{j=1}^{N} {}^{*}w_{k+1}^{(i)}}. \ \ (1 \le i \le N) \tag{9}$$

Next, compute effective sample size N_{eff}[12] as follows,

$$N_{eff} = \frac{1}{\sum_{i=1}^{N} {w_{k+1}^{(i)}}^2}. \tag{10}$$

The N_{eff} is introduced as a scale measuring how effectively particles are distributed. N_{eff}varies from 1 to N. When N_{eff} is 1, only one particle has a non-zero value, and all other particles have zero weights. When N_{eff} equals to N, weights of all particles are the same. The larger value N_{eff} means that the particles are effectively distributed to approximate the PDF.

Subsequently, only when N_{eff} falls below certain threshold N_τ, the following procedure is performed: samples particles $\{\boldsymbol{s}_{k+1|k+1}^{(i)}\}_{i=1}^{N}$ from $\{\boldsymbol{s}_{k+1|k}^{(i)}\}_{i=1}^{N}$ with replacement according to the weights $\{w_{k+1}^{(i)}\}_{i=1}^{N}$, and then set $\{w_{k+1}^{(i)}\}_{i=1}^{N}$ to 1. This procedure is called "resampling". The essence of this threshold-based algorithm is to avoid sample impoverishment by perform resampling only when N_{eff} is smaller value.

3.3. Merging Particle Filter

In order to overcome the sample impoverishment problem, a modification of the PF named Merging Particle Filter (MPF) was invented.[8] The MPF is one kind of particle filter, and the only different point between the MPF and the basic PF is in their resampling procedure. In the MPF-resampling, filtered ensemble is generated by *merging* the forecast ensemble. This process keeps diversity of particles and makes the MPF effective for the sample impoverishment problem.

The resampling step is explained as follows. Assume that the number of particles to be merged is n. Then sample N-particles $\{\boldsymbol{s}_{k+1|k}^{(i,j)}\}_{i=1}^{N}$ with replacement from forecast sub-ensemble $\{\boldsymbol{s}_{k+1|k}^{(i)}\}_{i=1}^{N}$. This procedure is performed for n times, and the sum of the sub-ensemble is $\{\{\boldsymbol{s}_{k+1|k}^{(i,j)}\}_{i=1}^{N}\}_{j=1}^{n}$. Note that each sub-ensemble must be sampled independently. Then, calculate the weighted sum of the n-particles, and make a new particle of the filtered ensemble, which is expressed as follows:

$$\boldsymbol{s}_{k+1|k+1}^{(i)} = \sum_{j=1}^{n} a_j \boldsymbol{s}_{k+1|k}^{(i,j)}, \tag{11}$$

where weights $\{a_j\}_{j=1}^{n}$ are chosen to satisfy following equations:

$$\sum_{j=1}^{n} a_j = 1, \ \ \sum_{j=1}^{n} a_j^2 = 1. \tag{12}$$

Satisfying Eq. (12) provides preservation of the mean and covariance of the PDF. By repeating this weighted-summing n times, the filtered ensemble $\{\boldsymbol{s}_{k+1|k}^{(i)}\}_{i=1}^{N}$ is generated. For the merging procedure to make sense, n must be equal or greater than 3.

When $n = 3$, setting a weight a_1 and inserting it into Eq. (12) determines a_2 and a_3 semi-uniquely. In this paper, n is set to be 3 for simplicity. Hereinafter, a_1 is referred to as m_p, which determines the characteristic of the MPF.

3.4. Implementation

The characteristic process in the proposed method is the following: putting each particle on the nearest asteroid surface (process A). When the asteroid surface is given as polygonal meshes, placing each particle to the nearest polygonal mesh corresponds to *process A*, for example. As it is clear from Eq. (11), filtering step of the MPF generates new particles which deviate from the asteroid surface. In order to satisfy the constraints that all particles exist on the asteroid surface, the deviated particles just after processed by Eq. (11) must be reallocated on the surface by *process A*. In this implementation, the filtered particles processed by the MPF-resampling and performing *process A* deviate from the real PDF. Iterative execution of both processes completely changes the PDF, which causes false approximation of the real PDF. In order to deal with this problem, setting N_τ to a smaller value is effective because this means reducing the number of the merging-resampling that causes the deviations. Also, setting m_p to be close to 1 is effective to mitigate this deviation.[13] For this purpose, in the following simulation, we set N_τ/N to 0.001, m_p to 0.9.

Despite the generality of this method, hereinafter the asteroid is assumed to be a sphere of radius ρ to evaluate the performance of the proposed method in the simple but typical case. In this case, the following process corresponds to *process A*,

$$\boldsymbol{X}_{k+1|k+1}^{(i)} \to \rho \frac{\boldsymbol{X}_{k+1|k+1}^{(i)}}{\|\boldsymbol{X}_{k+1|k+1}^{(i)}\|}, \tag{13}$$

which means scalar multiplying the vector $\boldsymbol{X}_{k+1|k+1}^{(i)}$ so that the norm becomes asteroid radius ρ.

The likelihood of each particle is computed as a product of each individual likelihood of measurement that is observable. The likelihoods of range measurement $P(\zeta_{rm}|\boldsymbol{s}^{(i)})$ and of camera based direction measurement are respectively calculated as

$$P(\zeta_{rm}|\boldsymbol{s}^{(i)}) = \frac{1}{\sqrt{2\pi\sigma_{rm}^2}} \exp\left\{-\frac{(h_{rm}(\boldsymbol{s}^{(i)}) - \zeta_{rm})^2}{2\sigma_{rm}^2}\right\}. \tag{14}$$

and

$$P(\boldsymbol{\zeta}_c|\boldsymbol{s}^{(i)}) = \frac{1}{2\pi\sqrt{\Sigma_c}} \exp\left\{-\frac{1}{2}(\boldsymbol{\zeta}_c - \boldsymbol{h}_c(\boldsymbol{s}^{(i)}))^T \Sigma_c (\boldsymbol{\zeta}_c - \boldsymbol{h}_c(\boldsymbol{s}^{(i)}))\right\}. \tag{15}$$

4. Simulation

4.1. Simulation parameters

The numerical simulations are performed for the following three methods, the conventional method based on the Kalman Filter (method A), the pure extension of the conventional method by using the MPF (method B), proposed method that uses the MPF considering the asteroid shape (method C). The conditions of the range measurement are set to be as follows. The observation interval is 100s and σ_{rm} = 3m, and only when

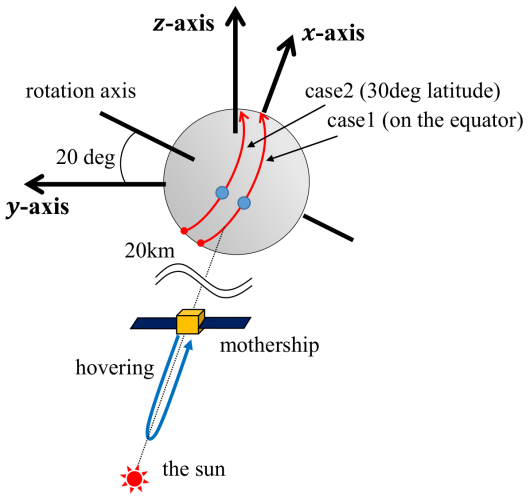

Fig. 2. Conceptual illustration of the simulations.

the directional angle θ is shorter than 80 deg, the range measurement is performed. θ is the angle between the vector from the lander to the mothership and the normal vector of the asteroid at the lander position. The conditions of the camera based asteroid direction measurement is set to be as follows: observation interval is 1800s and $\sigma_c = 0.1$ deg. The parameters σ_{rm} and σ_c are set to the same as Ref. 4) and Ref.11), respectively.

The initial position and velocity of the mothership are

$$\boldsymbol{x}_{0|0} = [-20000, 0, 0]^T \mathrm{m} \tag{16}$$

$$\boldsymbol{v}_{0|0} = [-\Delta V, 0, 0]^T \mathrm{m/s} \tag{17}$$

where ΔV is set to 0.0034 m/s so that the mothership comes back to the same height (20km) after 24 hours hovering period. The hovering altitude 20 km is the same as Hayabusa 2.[1)] Note that although the hovering operation in Hayabusa 2 is planned to be executed on the Earth-asteroid line, the hovering operation in our simulations is executed on the Sun-asteroid line for simplicity. The initial estimated position and velocity of the mothership are

$$\boldsymbol{x}_0 = \boldsymbol{x}_{0|0} + [100, 100, 100]^T \mathrm{m} \tag{18}$$

$$\boldsymbol{v}_0 = \boldsymbol{v}_{0|0} + [0.1, 0.05, 0.05]^T \mathrm{m/s} \tag{19}$$

In the following, we conducted the simulation for two cases. In case 1, the initial position of the lander is set to be on the equator of the asteroid. In case 2, the initial position of the lander set to be on 30 deg latitude location of the asteroid. The initial positions of the lander in case 1 and 2 are respectively expressed as follows,

$$\boldsymbol{X}_0 = [-84.4, 89.1, -417.3]^T \mathrm{m} \tag{20}$$

and

$$\boldsymbol{X}_0 = [-377.5, 213.1, 36.4]^T \mathrm{m}. \tag{21}$$

The initial estimated position of the lander is

$$\boldsymbol{X}_{0|0} = \boldsymbol{R}(\boldsymbol{\alpha}, \pi/4)\boldsymbol{X}_0. \tag{22}$$

The initial particle distribution of the lander position is assumed to follow a Gaussian with mean $\boldsymbol{X}_{0|0}$ and covariance matrix $(\mathrm{diag}(\boldsymbol{X}_{0|0} - \boldsymbol{X}_0))^2$. Since methods B and C use the MPF, the initial particles are scattered following the Gaussian above. The particle number of the MPF is set to $N = 500000$. The

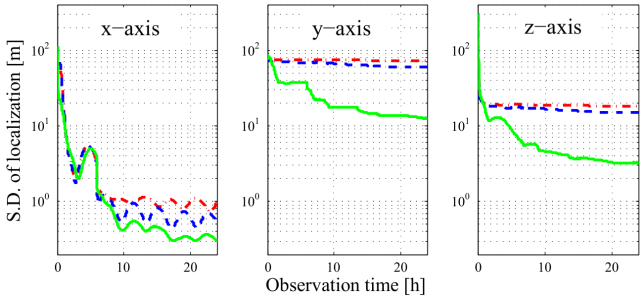

Fig. 3. The error standard deviations of each component of the lander position in case 1 are calculated by the methods A(red), B(blue), and C(green). The average values of 20 Monte Carlo trials are plotted.

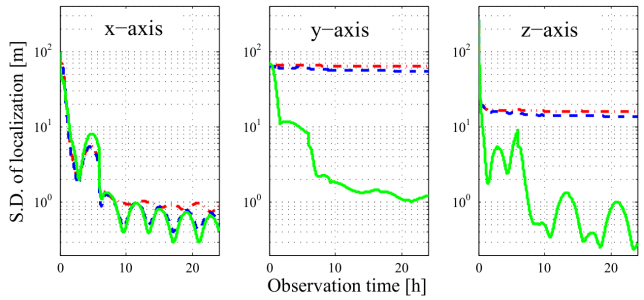

Fig. 4. The error standard deviations of each component of the lander position in case 2 are calculated by the methods A(red), B(blue), and C(green). The average values of 20 Monte Carlo trials are plotted.

value $N = 500000$ is large. However, it does not become a problem because the calculation itself is done on the ground in practical situation. In order to remove variations in the performance caused by the noise, the simulations were performed using Monte Carlo analysis by changing measurement noise for 20 times. The simulations were performed for 24 hours that equals to the period of the delta-V for hovering. The conceptual illustration of the simulations is shown in Fig. 2. Note that we set the operation day to November 8th 2018 so that the rotation axis of the asteroid is almost parallel to the y-z plane as shown in Fig. 2.

4.2. Simulation results

Figure 3 shows the comparison of standard deviations of the localization of the lander calculated by methods A, B, and C in cases 1. Figure 4 shows the comparison of standard deviations of the localization of the lander calculated by methods A, B, and C in cases 2. In both cases, method C provides the highest localization accuracy, followed in order by methods B and A. According to Figs. 3 and 4, the difference of the standard deviations in the y- and z-axes between methods A and B is relatively small, while the difference of those between the methods B and C is large. This result indicates that the high accuracy localization in the y- and z-axes by applying method C is not attributed to the efficacy of the MPF but to the consideration of the constraint of the asteroid surface.

The standard deviations of the localization in the y- and z-axes calculated by methods A and B take the similar values in cases 1 and 2. On the other hand, method C provides much better accuracy in the y- and z-axes in case 2 than in case 1. This difference can be explained as follows. When the x-directional uncertainty by one range measurement is given as Δx, the existence region of the lander obtained by that one time range

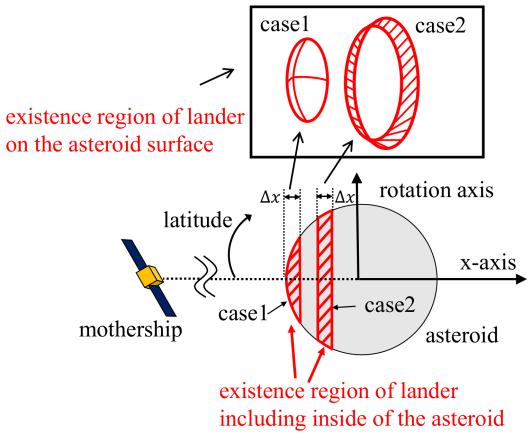

Fig. 5. The explanation of how method C works.

measurement is shown as the red shaded areas including inside of the asteroid as shown in Fig. 5. Methods A and B can not reduce the existence region anymore, while method C can do it. By considering the constraint that the lander exists on the asteroid surface, the existence regions of the lander can be reduced to the red shaded surface areas as shown in Fig. 5 (bowl shape for case 1 and onion ring shape for case 2). The red shaded surface areas are rotating around the rotation axis of the asteroid. Therefore, we can obtain those surfaces from different angles during the observation. Since, roughly speaking, the final existence region of lander is determined by the overlapping part of the surfaces obtained by all range measurements, it is clear that the overlapped red shaded surface area in case 2 becomes smaller than that in case 1. These things explain the higher localization accuracy in case 2 than in case 1. From the discussion above, we can expect that higher accuracy localization of the lander is achieved by applying method C when the lander exists in the higher latitude regions.

5. Conclusion

A localization method for asteroid lander from its mothership have been proposed by a previous research. However, since this conventional method relies on the changes of the direction from the mothership to the lander in the orbiting operation of the mothership, it does not work well in the case when the directional change is small. One of such cases is the hovering operation that is chosen by Hayabusa and Hayabusa 2 missions as a nominal operation. In order to make the conventional method applicable in the general cases, we proposed the improved filtering method that takes into account the constraints that the lander exists on the asteroid surface. The simulation results show the superiority of the proposed method over the conventional one in the hovering operation. Also, the simulation results indicate that the proposed method demonstrates the superiority over the conventional method especially when the lander exists in the high latitude region of the asteroid.

References

1) Tsuda, Y., Yoshikawa, M., Abe, M., Minamino, H., and Nakazawa, S.: System design of the Hayabusa 2-asteroid sample return mission to 1999 JU3, *Acta Astronautica*., **91**(2013), pp. 356–362.
2) Pavone, M., Castillo-Rogez, J. C., Nesnas, I. A., Hoffman, J. A., and Strange, N. J.: Spacecraft/Rover hybrids for the exploration of small solar system bodies, Aerospace Conference, 2013 IEEE (pp. 1-11). IEEE.
3) Yoshimitsu, T., Kubota, T., Nakatani, I., Adachi, T., and Saito, H.: Micro-hopping robot for asteroid exploration, *Acta Astronautica*., **52**(2003), pp. 441–446.
4) Kanata, S., Nakanishi, H., Sawaragi, T., Yoshimitsu, T., and Nakatani, I.: Radio Wave Based Localization of a Rover for a Small Planetary Body, *Journal of the Robotics Society of Japan*, **27**(2009), pp. 1007–1015 (in Japanese).
5) Kawaguchi, J. I., Fujiwara, A., and Uesugi, T.: Hayabusa-its technology and science accomplishment summary and Hayabusa-2, *Acta Astronautica*, **62**(2008), pp. 639–647.
6) Gaskell, R., Barnouin-Jha, O., Scheeres, D., Mukai, T., Hirata, N., Abe, S., ... and Kawaguchi, J.: Landmark navigation studies and target characterization in the Hayabusa encounter with Itokawa, AIAA/AAS Astrodynamics Specialist Conference and Exhibit (p. 6660).
7) Yoshimitsu, T., Tomiki, A., and Kubota, T.: Proposal of range measurement experiment using a balloon, 2015 Symposium on balloon, 2015 (in Japanese).
8) Nakano, S., Ueno, G., and Higuchi, T.: Merging particle filter for sequential data assimilation, *Nonlinear Processes in Geophysics*, **14**(2007), pp. 395–408.
9) Kikuchi, S., Tsuda, Y., and Kawaguchi, J.: Stabilization Strategy of Delta-V Assisted Periodic Orbits around Asteroids Based on an Augmented Monodromy Matrix, *Trans. JSASS Aerospace Technology Japan*, **14**, ists30 (2016), pp.Pd_85–Pd_94.
10) Bellerose, J., and Hajime, Y.: Dynamics of asteroid 1999 JU3: Target of the Hayabusa follow-on mission, *Trans. JSASS Aerospace Technology Japan*, **7**, ists26 (2010), pp.Tk_23–Tk_28.
11) Kikuchi, S., Tsuda, Y., and Kawaguchi, J.: Delta-V Assisted Periodic Orbits Around Small Bodies, *Journal of Guidance, Control, and Dynamics*., **40**(2017), pp. 150–163.
12) Kong, A., Lui, J. S., and Wong, W. H. (1994).: Sequential imputation and Bayesian missing data problems. *Journal of the American statistical association*., **89**(1994), pp. 278–288.
13) Nakano, S., Ueno, G., Nakamura, K., and Higuch, T.: Merging Particle Filter and Its Characteristics, *Proceeding of the Institute of Statistical Mathematics*, **56**(2008), pp. 225-234 (in Japanese).